Journal of Histochemistry & Cytochemistry 2018, Vol. 66(3) 175–187

DOI: 10.1369/0022155417749491
journals.sagepub.com/home/jhc
SAGE

Expression and Cellular Localization of IFITM1 in Normal and Injured Rat Spinal Cords

Ying Wang*, Yu-Hong Lin*, Yan Wu*, Zong-Feng Yao, Jie Tang, Lin Shen, Rui Wang, Shu-Qin Ding, Jian-Guo Hu, and He-Zuo Lü

Clinical Laboratory (YIW, Y-HL, YAW, Z-FY, S-QD, J-GH, H-ZL) and Anhui Key Laboratory of Tissue Transplantation (YIW, Y-HL, YAW, Z-FY, JT, LS, RW, J-GH, H-ZL), The First Affiliated Hospital of Bengbu Medical College, Bengbu, P.R. China, and Department of Immunology (Y-HL, YAW, JT, H-ZL) and Anhui Key Laboratory of Infection and Immunity (Y-HL, YAW, JT, H-ZL), Bengbu Medical College, Bengbu, P.R. China

Summary

Interferon-induced transmembrane protein 1 (IFITM1) is a member of the IFITM family that is associated with some acute-phase cytokine-stimulated response. Recently, we demonstrated that IFITM1 was significantly upregulated in the injured spinal cords at the mRNA level. However, its expression and cellular localization at the protein level is still unclear. Here, a rat model of spinal cord injury (SCI) was performed to investigate the spatio-temporal expression of IFITM1 after SCI. IFITM1 mRNA and protein were assessed by quantitative reverse transcription-PCR and western blot, respectively. IHC was used to identify its cellular localization. We revealed that IFITM1 could be found in sham-opened spinal cords and gradually increased after SCI. It reached peak at 7 and 14 days postinjury (dpi) and still maintained at a relatively higher level at 28 dpi. IHC showed that IFITM1 expressed in $GFAP^+$ and APC^+ cells in sham-opened spinal cords. After SCI, in addition to the above-mentioned cells, it could also be found in $CD45^+$ and $CD68^+$ cells, and its expression in $CD45^+$, $CD68^+$, and $GFAP^+$ cells was increased significantly. These results demonstrate that IFITM1 is mainly expressed in astrocytes and oligodendroglia in normal spinal cords, and could rapidly increase in infiltrated leukocytes, activated microglia, and astrocytes after SCI. (J Histochem Cytochem 66:175–187, 2018)

Keywords

astrocytes, expression, IFITM1, infiltrated leukocytes, microglia, spinal cord injury

Introduction

Spinal cord injury (SCI) is damage to the spinal cord that results in devastating loss of motor and sensory functions. In the United States, it is reported that ~300,000 people are living with SCI, and nearly 12,000 new patients are diagnosed annually.[1] In China, the incidence of traumatic SCI is approximately 60,000 per year.[2] Although there are some advances in surgical techniques of the spinal cord, there still are no effective treatments for this devastating neurological disorder.[3] Therefore, it is very important to further understand the molecular mechanisms of SCI.

Received for publication September 28, 2017; accepted November 17, 2017.

*These authors contributed equally to this work.

Corresponding Authors:
He-Zuo Lü, Anhui Key Laboratory of Tissue Transplantation, The First Affiliated Hospital of Bengbu Medical College, 287 Chang Huai Road, Bengbu 233004, P.R. China.
E-mail: lhz233003@163.com

Jian-Guo Hu, Anhui Key Laboratory of Tissue Transplantation, The First Affiliated Hospital of Bengbu Medical College, 287 Chang Huai Road, Bengbu 233004, P.R. China.
E-mail: jghu9200@163.com

Journal of Histochemistry & Cytochemistry

Recently, we demonstrated that interferon-induced transmembrane protein 1 (IFITM1) was significantly upregulated in injured spinal cords at the mRNA level by using RNA-sequencing.[4] IFITM1, also known as Leu 13, 9–27 or interferon (IFN) inducible protein 17, is associated with the transduction of homotypic adhesion and antiproliferative signals in lymphocytes.[5,6] It is required for the progression of cancers by enhancing their proliferation, migration, and invasion.[7–10] It is also involved in the physiological process of primordial germ cell development.[11,12] Some studies reported that IFITM1 is expressed in a variety of tissues and cells, and its expression level can be significantly increased by stimulation of IFNs and some acute-phase cytokines.[13,14] However, its spatio-temporal expression at the protein level in injured spinal cords is still unclear. In this study, we performed an SCI model in adult Sprague-Dawley rats and investigated the expression pattern of IFITM1. Quantitative reverse transcription q(RT)-PCR and western blot were used to assess its expression at the mRNA and protein level, respectively. IHC analysis was used to identify which cell types are expressing this protein.

Materials and Methods

Animals

A total of 108 9-week-old female Sprague-Dawley rats (220–250 g, Vital River Laboratory Animal Technology Co. Ltd.; Beijing, China) were used in this study. The animal care in the surgical procedures and after operation were in accordance with the Regulations for the Administration of Affairs Concerning Experimental Animals (Ministry of Science and Technology, China; revised in June 2004) and the Guide for the Care and Use of Laboratory Animals and the Guidelines and Policies for Rodent Survival Surgery approved by the Animal Care and Ethics Committees of Bengbu Medical College.

Contusive SCI

Contusive SCI was performed using a New York University Impactor as previously described.[15] Briefly, rats were anesthetized with pentobarbital (50 mg/kg, intraperitoneal) and received a laminectomy at T9 vertebra. To make the contusive injury, the T7 and T11 vertebrae were clamped to stabilize the spine, and the exposed dorsal surface of the cord was subjected to a weight drop injury using a 10 g rod (2.5 mm diameter) dropped at a height of 25 mm. Sham-operated (sham) rats only received a laminectomy without contusive injury. After surgery, muscles and skin were closed in layers, and rats were placed in a temperature- and humidity-controlled chamber. The analgesic agent, buprenorphine (0.05 mg/kg, SQ; Reckitt Benckise; Hull, England) was used every 12 hr for 3 consecutive days. Manual bladder emptying was performed 3 times daily until reflex bladder emptying was established. To prevent infections, animals were daily provided with chloramphenicol (~50–75 mg/kg) via drinking water.

RNA Extraction and Real-Time RT-PCR

Immediately after euthanasia with an overdose of sodium pentobarbital (80 mg/kg, intraperitoneal), the rats were perfused with 200 ml saline. The spinal cords (1 cm spinal cord segment) of sham, and the spinal cords (1 cm spinal cord segment containing the injury epicenter) of acute (1 and 3 dpi), subacute (7 and 14 dpi), and chronic phases (28 dpi) were harvested (n=6 in every group). The total RNA from the spinal cords was extracted using TRIzol reagent (Invitrogen; New Jersey, NJ) according to the manufacturer's instructions. RNA was reverse transcribed into cDNA using a reverse transcription system (Promega; Madison, WI). Real-time PCR was performed on an ABI 7900 PCR detection system (Applied Biosystems; Foster City, CA) using a SYBR Green PCR Master Mix (Applied Biosystems). Parallel amplification of the β-*actin* housekeeping gene was used to normalize gene expression. The primer sequences were IFITM1 forward primer 5′-TCGGACCAAGCCTGTATCCT-3′; IFITM1 reverse primer 5′-GATTGTGGTGGTTGTCGCAG-3′; β-actin forward primer 5′-AAGTCCCTCACCCTCCCAAAAG-3′; and β-actin reverse primer 5′-AAGCAATGCTGTC ACCTTCCC-3′. The relative expression level of target mRNAs was calculated using the $^{\Delta\Delta}$Ct method[16] and expressed relative to the value in the vehicle group (designated as 1).

Western Blot Analysis

Immediately after euthanasia with an overdose of sodium pentobarbital (80 mg/kg, intraperitoneal), the rats were perfused with 200 ml saline. The spinal cord segment (T8–T10) was dissected for detecting the expression of IFITM1 in sham and injured spinal cord. The spinal cords were homogenized in a lysis buffer containing 50 mM Tris-HCl, 150 mM NaCl, 1% NP-40, 0.5% sodium deoxycholate, 0.1% sodium dodecyl sulfate, 1 mM EDTA, 1 mM sodium orthovanadate, 10 mM sodium fluoride, 4 µg/ml leupeptin, 1 µg/ml aprotinin, and 100 µg/ml PMSF (all from Sigma). The supernatant was clarified by centrifugation at 16,000 g for 10 min at 4C. The protein concentrations of the lysates were determined using a bicinchoninic acid

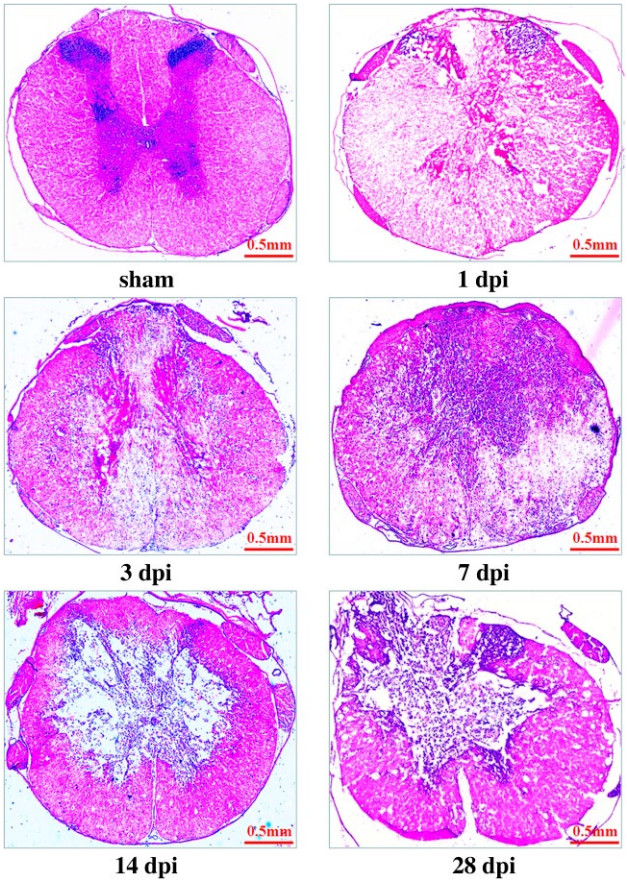

Figure 1. Histopathological changes after SCI evaluated by H&E staining. The pictures of whole coronal sections of the spinal cords were evaluated by H&E staining. The spinal cords come from different stages of SCI: sham, 1, 3, 7, 14, and 28 dpi. Scale bars = 0.5 mm. Abbreviations: SCI, spinal cord injury; dpi, days postinjury.

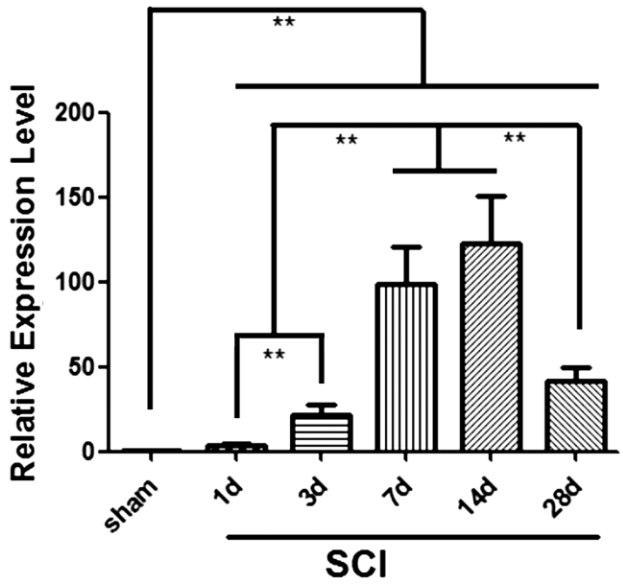

Figure 2. The mRNA expression of IFITM1 in injured spinal cords. The mRNA expression of IFITM1 in injured spinal cords was measured by using real-time RT-PCR. Its relative expression level was calculated using the $^{\Delta\Delta}$Ct method and expressed relative to the value in the sham group (designated as 1). Abbreviations: IFITM1, interferon-induced transmembrane protein 1; RT-PCR, reverse transcription PCR; SCI, spinal cord injury. Data represent the mean ± SD (n=6). **p<0.01 (ANOVA).

(BCA) Protein Assay kit (Pierce; Rockford, IL). For western blotting, supernatants were diluted in sample buffer (62.5 mM Tris–HCl, pH 6.8, 2% SDS, 10% glycerol, 50 mM Dithiothreitol (DTT), and 0.1% bromophenol blue) and boiled for 5 min. Equal amounts of protein (20 µg) were resolved on 8% SDS-polyacrylamide gel electrophoresis and transferred to polyvinylidene difluoride membranes (Millipore; Bedford, MA). The membranes were blocked at room temperature for 1 hr in 5% (w/v) dry skim milk in TBS plus 0.1% Tween-20 (TBST), rinsed in TBST and incubated with primary antibodies at 4C overnight. Primary antibodies used were rabbit anti-beta-actin (1:2000, cat no. BL005B, Biosharp; China) and rabbit anti-IFITM1 (1:500, cat no. 251403; ABBIOTEC; San Diego, CA). After being rinsed with TBST, the membranes were incubated with the appropriate horseradish peroxidase (HRP)-conjugated secondary antibody (KPL; Gaithersburg, MD) for 1 hr at room temperature. To visualize the immunoreactive proteins, the enhanced chemiluminescence (ECL) kit (Pierce) was used following the manufacturer's instructions. Films were digitized and densitometry was performed using Gel-Pro analyzer (Media Cybernetics; Silver Spring, MD).

IHC

After the indicated time periods postinjury, animals were euthanized with an overdose of sodium pentobarbital (nembutal; 80 mg/kg, interperitoneal) and perfused with 200 ml physiological saline followed by fixation with 300 ml ice-cold 4% paraformaldehyde (PFA) in 0.01 M PBS (pH 7.4). After perfusion, a 1 cm spinal cord segment containing the injury epicenter was removed, postfixed overnight in 4% PFA in 0.01 M PBS (pH 7.4), and transferred to 30% sucrose in 0.01 M PBS (pH 7.4) at 4C overnight. Then, the segments were placed in optimal cutting temperature (OCT) compound embedding medium (Tissue-Tek; Miles, Elkart, IN) and 8 µm frozen sections were obtained transversely using a cryostat (Leica CM1900; Bannockburn, IL), followed by thaw-mounting on poly-L-lysine-coated slides (Sigma). For IHC, the sections were blocked with 10% normal goat serum (NGS) in

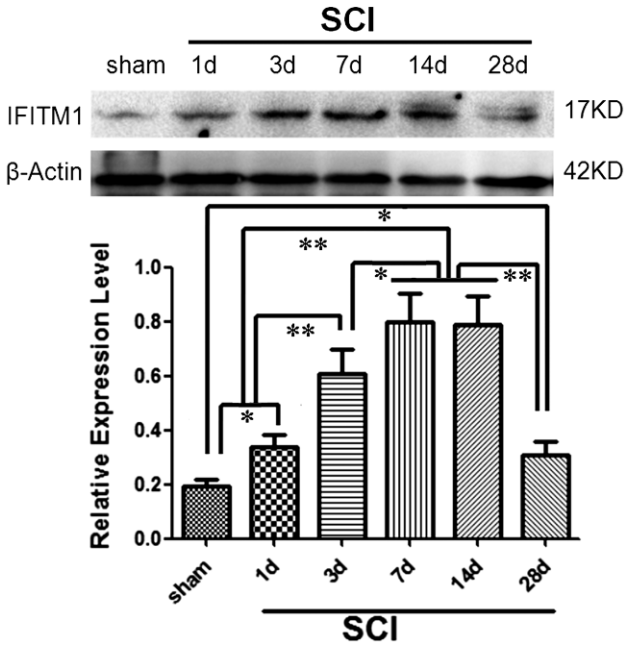

Figure 3. Expression of IFITM1 protein after SCI detected by western blot. The upper figure shows the representative western blot images of *IFITM1* (17 kDa) and housekeeping gene *β-actin* (42 kDa). Band densities were quantified using Gel-Pro analyzer software. The ratio of IFITM1/*β*-actin band density from blots was used to quantify the expression level of the IFITM1 protein. Housekeeping protein β-actin was used as the internal control. The lower statistical graph shows the IFITM1 protein levels in sham and injured spinal cords at 1, 3, 7, 14, and 28 dpi. Abbreviations: IFITM1, interferon-induced transmembrane protein 1; SCI, spinal cord injury; dpi, days postinjury. Data represent the mean ± SD (n=6). $^{**}p<0.01$, $^{*}p<0.05$ (ANOVA).

0.01 M PBS (pH 7.4) for 1 hr. And then, the primary rabbit anti-rat IFITM1 (1:70, cat. no 251403; ABBIOTEC) was applied overnight at 4C with mouse anti-rat CD45 (1:200; cat. no MCA43R; AbD Serotech; Oxford, UK), mouse anti-rat CD68 (1:200; cat. no MCA341GA; RRID: AB_566872; AbD Serotech); mouse anti-rat glial fibrillary acidic protein (GFAP, 1:200; cat. no G3893; Sigma-Aldrich); mouse anti-adenomutons polyposis coli gene Chr 5q (APC) antibody [CC-1] (1:100; cat. no ab16794; Abcam; Cambridge, UK); and mouse anti-neuron-specific nuclear protein (NeuN) antibody [1B7]—Neuronal Marker (1:100; cat. no ab104224; Abcam), respectively. The following day, sections were incubated for 60 min at 37C with FITC-conjugated goat anti-mouse (1:200; cat. no 115-095-003; RRID: AB_2338589; Jackson Immuno Research Lab.; West Grove, PA) and rhodamine-conjugated goat anti-rabbit antibodies (1:200; cat. no 111-025-144; RRID: AB_2337932; Jackson Immuno Research Lab.). The coverslips were rinsed and mounted with mounting media containing Hoechst 33342, a nuclear dye (0.5 μM, Sigma). The results of the immunostaining were examined with a ZEISS Axio Observer microscope. The quantitative analysis was performed by using the ImageJ Software (http://rsb.info.nih.gov/ij/; National Institutes of Health).[17,18] For cells with regular shapes, such as leukocytes and microglia, we evaluated them quantitatively using the number of positive cells. For irregularly shaped cells, such as neurons and astrocytes, we evaluated them quantitatively using cell fluorescence density. For determining the cell fluorescence density, the multiple-color channels in immunofluorescence-labeled images were split by running Image–>Color–>Split Channels. The images of different channels were converted to 8-bit grayscale. Then, the semi-automated cell density measuring was performed according to Drury's method.[18] Briefly, cells were identified using a manual threshold (Image–>Adjust–>Threshold) followed by running Process–>Binary–>Watershed to generate a visual array in which each cell was colored white and the non-cellular material black. Select the region of interest using the drawing tools. Select "set measurements" from the Analyze menu and make sure "Area," "Integrated density," and "Limit to threshold" are selected. Select Image–>Adjust–>Threshold to make the cells in the picture just all is selected. Select "Set Scale" from the analyze menu, and enter "pixels" in the box on the edge of "Unit of length." Finally, select "Measure" from the analyze menu. A popup box with a stack of values will be seen. In the popup box, IntDen is the abbreviation of "integrated density," which means the sum over all calibrated pixel values. The value of IntDen divided by the area to be analyzed indicates the fluorescence density of the cell to be measured. The cell number or fluorescence density was calculated by 2 blinded observers in a set of 5 sections, from rostral to caudal in cross-sections of 1 cm spinal cord containing the injury epicenter.

Statistical Analyses

Statistical values are presented as mean ± SD. Normal distribution was analyzed to justify the ANOVA can be used. The data were analyzed using two-way ANOVA, followed by Bonferroni post hoc test for comparisons between groups. Statistical differences were considered significant at $p<0.05$.

Results

Histopathological Changes After SCI

To observe the histopathological changes after SCI, H&E staining was performed. As shown in Fig. 1, in spinal cord transverse sections of sham group, the gray matter and white matter were complete. However,

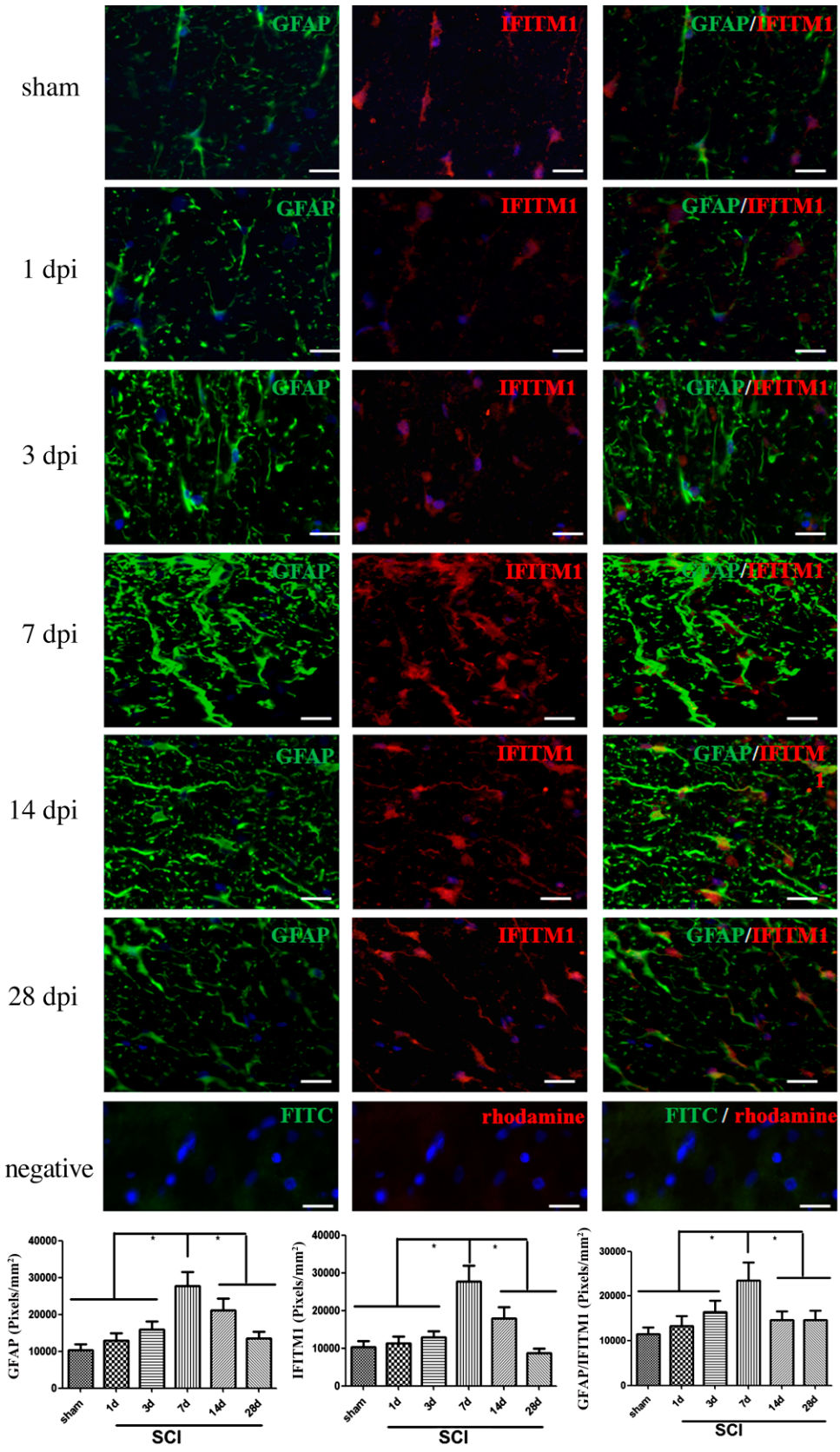
sham
1 dpi
3 dpi
7 dpi
14 dpi
28 dpi
negative
GFAP
IFITM1
GFAP/IFITM1
FITC
rhodamine
FITC / rhodamine
GFAP (Pixels/mm²)
IFITM1 (Pixels/mm²)
GFAP/IFITM1 (Pixels/mm²)
sham
1d
3d
7d
14d
28d
SCI

(continued)

Figure 4. Co-localization of IFITM1 with GFAP in spinal cords after SCI. Representative images of GFAP (green) and IFITM1 (red) immunostaining in the spinal cords of sham-opened, 1, 3, 7, 14, and 28 dpi. The nuclei were counterstained by using Hoechst 33342 (blue). The lower statistical graphs show the density of $GFAP^+$ $IFITM1^+$ and $GFAP^+$ $IFITM1^+$ cells in sham and injured spinal cords at 1, 3, 7, 14, and 28 dpi. The micrographs were located at peripheral white matter in the sham group, and white matter spared near the injury epicenter at the cross-sections within 1 mm distance from injury center in SCI groups. Scale bars = 20 μm. Abbreviations: IFITM1, interferon-induced transmembrane protein 1; GFAP, glial fibrillary acidic protein; SCI, spinal cord injury; dpi, days postinjury. Data represent the mean ± SD (n=6). *p<0.05 (ANOVA).

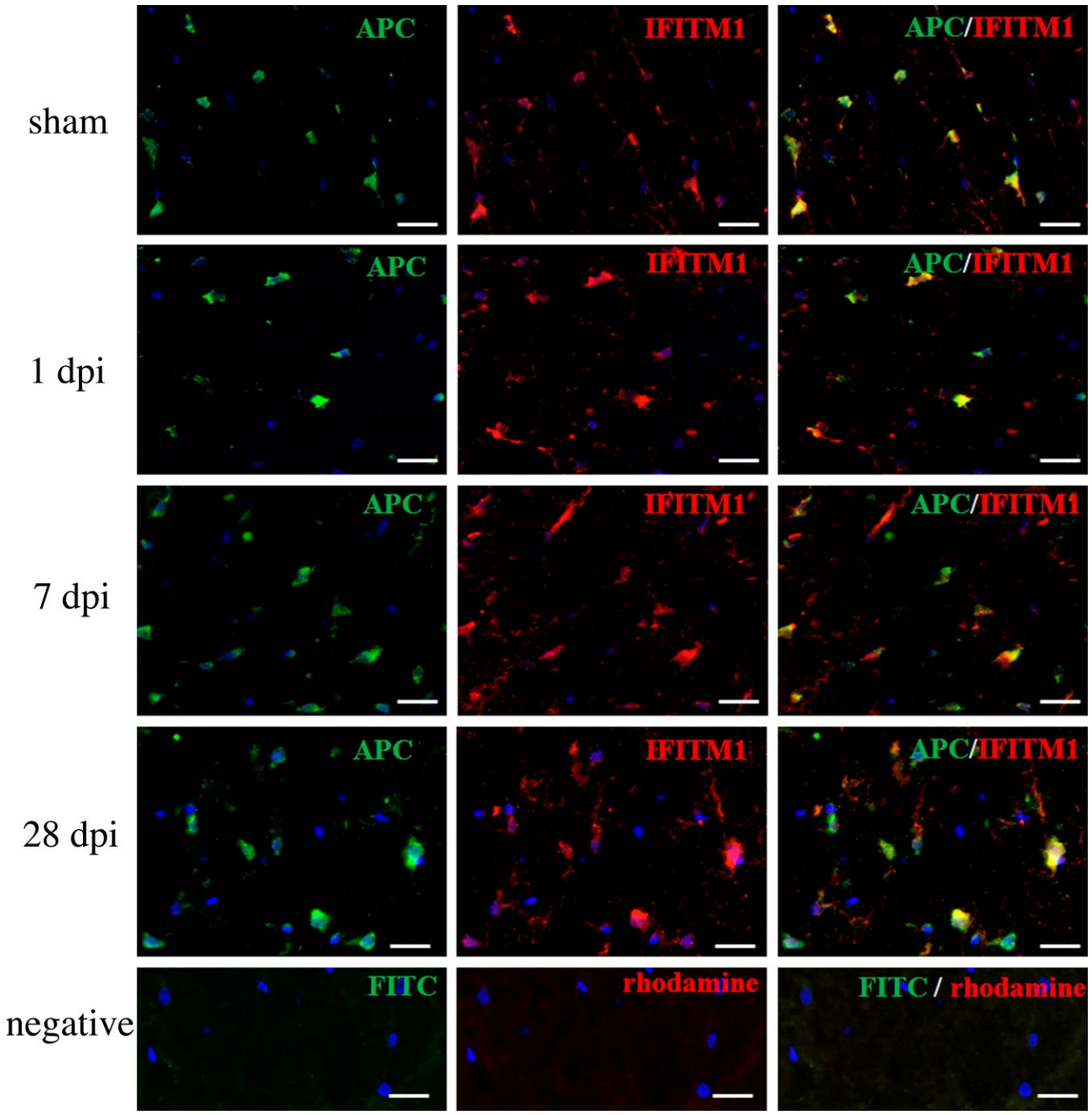

Figure 5. Co-localization of IFITM1 with APC in spinal cords after SCI. Representative images of APC (green) and IFITM1 (red) immunostaining in the spinal cords of sham-opened, 1, 7, and 28 dpi groups. The nuclei were counterstained by using Hoechst 33342 (blue). The micrographs were located at peripheral white matter in the sham group, and white matter spared near the injury epicenter at the cross-sections 5 mm distance from the injury center in SCI groups. Scale bars = 20 μm. Abbreviations: APC, adenomutons polyposis coli gene Chr 5q; IFITM1, interferon-induced transmembrane protein 1; SCI, spinal cord injury; dpi, days postinjury.

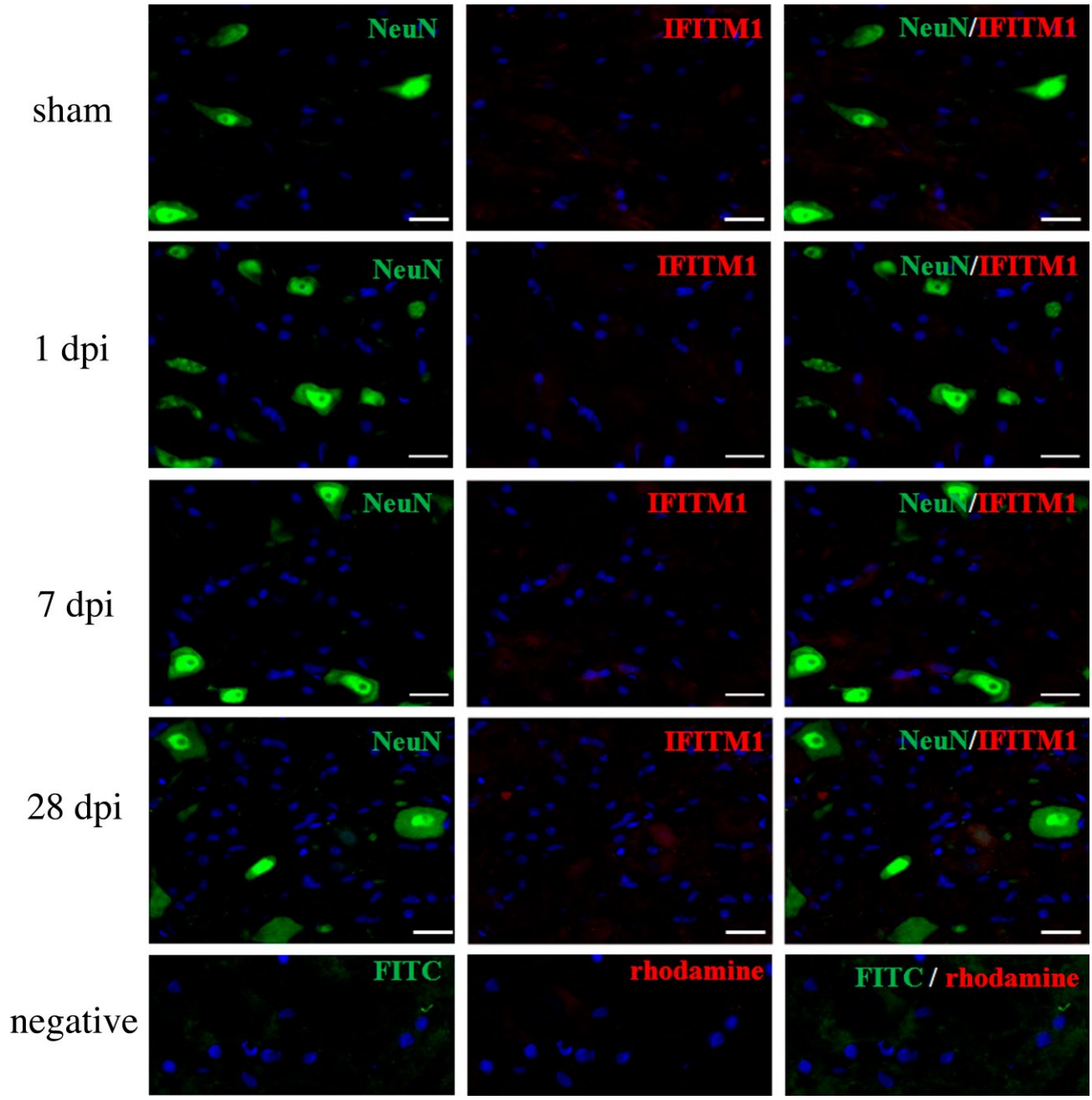

Figure 6. Co-localization of IFITM1 with NeuN in spinal cords after SCI. Representative images of NeuN (green) and IFITM1 (red) immunostaining in the spinal cords of sham-opened, 1, 7, and 28 dpi groups. The nuclei were counterstained by using Hoechst 33342 (blue). The micrographs come from gray matter at the cross-sections 5 mm distance from the injury center. Scale bars = 20 μm. Abbreviations: IFITM1, interferon-induced transmembrane protein 1; SCI, spinal cord injury; dpi, days postinjury; NeuN, neuron-specific nuclear protein.

in the contusion groups (1, 3, 7, 14, and 28 dpi), we could find the loss of neurons and glias in the injury epicenter and a rim of peripheral spared white matter. There were also a large number of infiltrated inflammatory cells in the injury epicenter. In addition, the boundary between the injury center and the peripheral residual tissue gradually became clear with the extension of injury time. These were the typical histopathological changes of the SCI contusion model in rats.

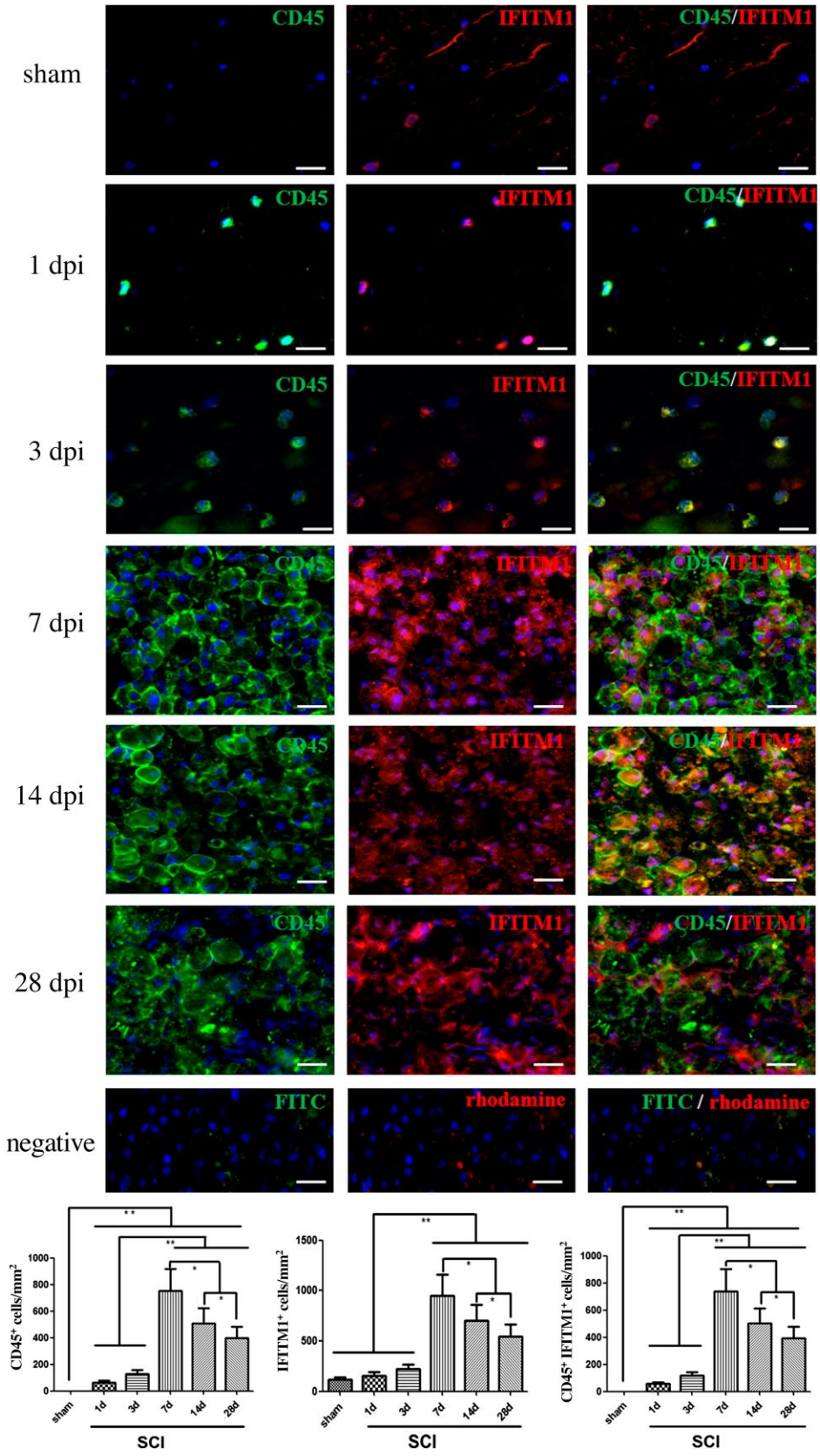
sham
1 dpi
3 dpi
7 dpi
14 dpi
28 dpi
negative
CD45
IFITM1
CD45/IFITM1
FITC
rhodamine
FITC / rhodamine
CD45+ cells/mm2
IFITM1+ cells/mm2
CD45+ IFITM1+ cells/mm2
sham
1d
3d
7d
14d
28d
SCI

(continued)

Figure 7. Co-localization of IFITM1 with CD45 in spinal cords after SCI. Representative images of CD45 (green) and IFITM1 (red) immunostaining in the spinal cords of sham-opened, 1, 3, 7, 14, and 28 dpi. The nuclei were counterstained by using Hoechst 33342 (blue). The lower statistical graphs show the number of $CD45^+$ $IFITM1^+$ and $CD45^+$ $IFITM1^+$ cells in sham and injured spinal cords at 1, 3, 7, 14, and 28 dpi. The micrographs were located at white matter adjacent to the gray matter in sham group, and white matter in the injury epicenter of the cross-sections within 1 mm distance from injury center in SCI groups. Scale bars = 20 μm. Abbreviations: IFITM1, interferon-induced transmembrane protein 1; SCI, spinal cord injury; dpi, days postinjury. Data represent the mean ± SD (n=6). $^{**}p<0.01$, $^{*}p<0.05$ (ANOVA).

The mRNA Expression of IFITM1 in Injured Spinal Cord Tissue

The mRNA expression of IFITM1 in the injured spinal cord was analyzed by real-time RT-PCR. As shown in Fig. 2, the mRNA expression of IFITM1 could be detected in the tissue samples from each group. However, tissue samples from the injured groups had higher mRNA expression as compared with the sham group ($p<0.01$). There was also significant difference among the injured groups: the IFITM1 mRNA levels in 7 and 14 dpi were significantly higher than those in any other groups ($p<0.01$); the levels in 3 and 28 dpi groups were also significantly higher than that in 1 dpi group ($p<0.01$).

Expression of IFITM1 Protein in Injured Spinal Cord Tissue

The expression of IFITM1 at the protein level in sham and injured spinal cords was detected by western blot. As shown in Fig. 3, there was weak expression of the IFITM1 protein in the sham-opened group. After SCI, it gradually increased, reached a peak at 7 and 14 dpi; although it was decreased up to 28 dpi (the longest time evaluated in this study), it still maintained at a higher level. The statistical graph showed that the IFITM1 protein levels in all injured groups were significantly higher than those in the sham-opened group (1 and 28 dpi vs. sham: $p<0.05$; 3, 7, and 14 dpi vs. sham: $p<0.01$). The IFITM1 protein levels in 3, 7, and 14 dpi were also significantly higher than those in the other three groups ($p<0.01$). There were no significant differences between the 7 and 14 dpi groups ($p>0.05$), but there were significant differences among 3 dpi, 7 dpi, and 14 dpi groups. The levels in 7 and 14 dpi were significantly higher than that in the 3 dpi group ($p<0.05$).

Cellular Localization of IFITM1 in Injured Spinal Cord Tissue

To further address the cellular localization of IFITM1 in the spinal cords, double-immunofluorescence staining of IFITM1 and the other cell markers was used in transverse cryosections of spinal cord tissues. Because a large number of neurons and oligodendroglia were lost in the injury center, we used the sections 5 mm distance from the injury center to co-localize them with IFITM1. The sections within 1 mm distance from the injury center were used for co-localization of IFITM1 with the other cells. Because different types of cells are distributed in different regions, to clarify the co-localization of IFITM1 with them in cross-sections, different regions were chosen. GFAP and APC were viewed at peripheral white matter in the sham group, and white matter spared near the injury epicenter in SCI groups. CD45 and CD68 were viewed at the white matter adjacent to the gray matter in the sham group, and white matter in the injury epicenter. NeuN was viewed at white matter in all groups. The results showed that IFITM1 was found in $GFAP^+$ (Fig. 4) and APC^+ (Fig. 5), but not $NeuN^+$ (Fig. 6) cells in the sham-opened spinal cords. No $CD45^+$ (Fig. 7) and $CD68^+$ (Fig. 8) cells were found in the sham-opened spinal cords. After SCI, in addition to $GFAP^+$ (Fig. 4) and APC^+ (Fig. 5) cells, IFITM1 could also be almost found in both $CD45^+$ (Fig. 7) and $CD68^+$ (Fig. 8) cells. However, its expression in $NeuN^+$ (Fig. 6) was very rare. The densities of APC^+ $IFITM1^+$ and APC^+ $IFITM1^+$ cells (Fig. 5) in sham-opened and all injured groups had no statistically significant differences (data not shown). Statistical results showed that the densities of $GFAP^+$ $IFITM1^+$ and $GFAP^+$ $IFITM1^+$ cells (Fig. 4) were higher in the 7 dpi group than those of the other groups ($p<0.05$). The quantities of $CD45^+$ $IFITM1^+$ and $CD45^+$ $IFITM1^+$ cells (Fig. 7), and $CD68^+$ $IFITM1^+$ and $CD68^+$ $IFITM1^+$ cells (Fig. 8) had similar trends. They were gradually increased after injury, reached the peaks at 7 dpi, and maintained at higher levels for up to 28 dpi ($p<0.05$ or 0.01).

Discussion

In this study, we performed an SCI model in adult Sprague-Dawley rats and investigated the expression pattern of IFITM1 after injury. Quantitative RT-PCR, western blot, and IHC analysis revealed that IFITM1 could be detected in sham-opened spinal cords. After SCI, it gradually increased, reached a peak at 7 and 14 days postinjury (dpi); although it

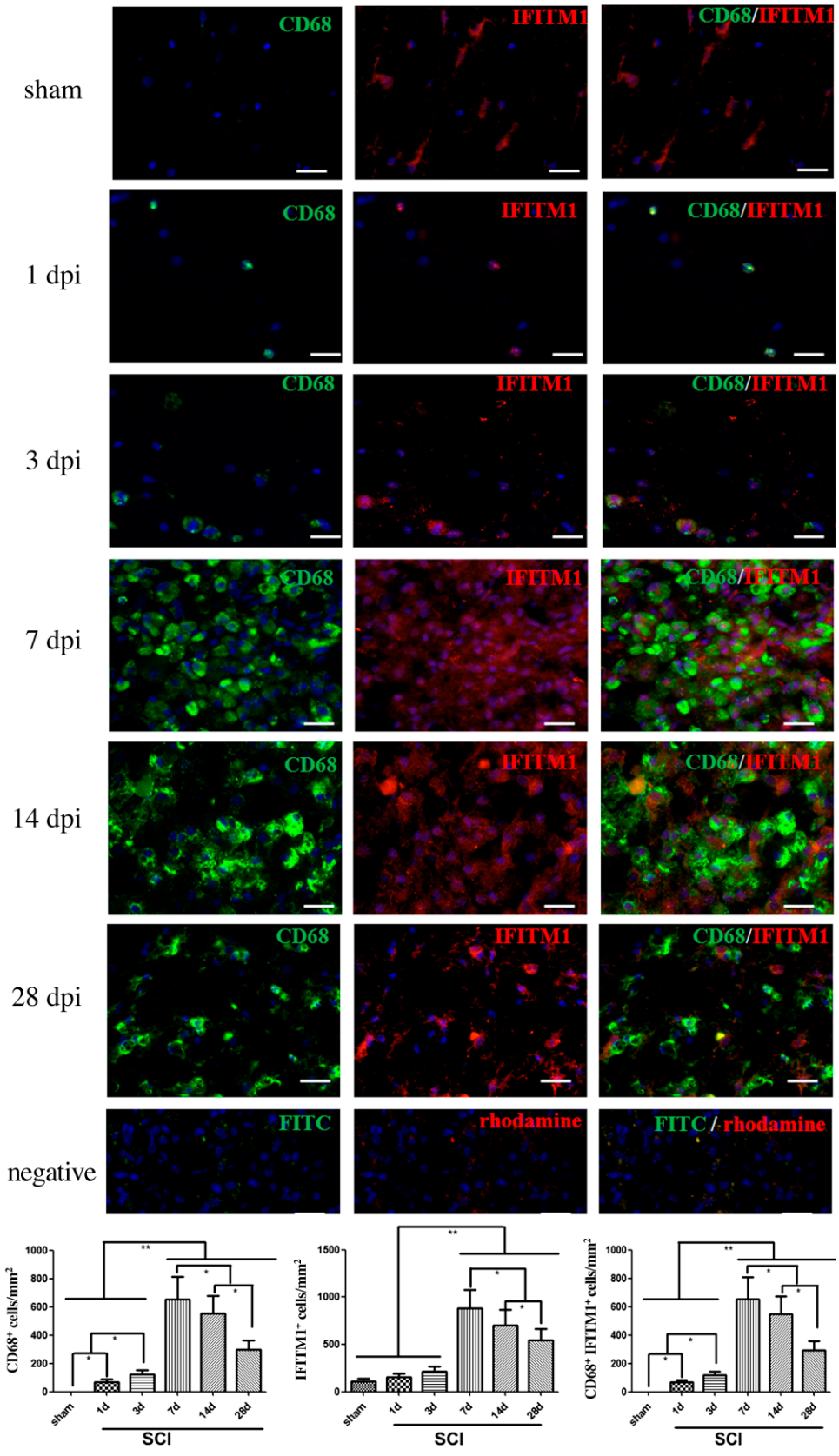
sham
1 dpi
3 dpi
7 dpi
14 dpi
28 dpi
negative
CD68
IFITM1
CD68/IFITM1
FITC
rhodamine
FITC / rhodamine
CD68+ cells/mm2
IFITM1+ cells/mm2
CD68+ IFITM1+ cells/mm2
sham
1d
3d
7d
14d
28d
SCI

(continued)

Figure 8. Co-localization of IFITM1 with CD68 in spinal cords after SCI. Representative images of CD68 (green) and IFITM1 (red) immunostaining in the spinal cords of sham-opened, 1, 3, 7, 14, and 28 dpi. The nuclei were counterstained by using Hoechst 33342 (blue). The lower statistical graphs show the number of $CD68^+$ $IFITM1^+$ and $CD68^+$ $IFITM1^+$ cells in sham and injured spinal cords at 1, 3, 7, 14, and 28 dpi. The micrographs were located at the white matter adjacent to the gray matter in the sham group, and white matter in the injury epicenter of the cross-sections within 1 mm distance from injury center in SCI groups. Scale bars = 20 μm. Abbreviations: IFITM1, interferon-induced transmembrane protein 1; SCI, spinal cord injury; dpi, days postinjury. Data represent the mean ± SD (n=6). $^{**}p<0.01$, $^{*}p<0.05$ (ANOVA).

was decreased up to 28 dpi (the longest time evaluated in this study), it still maintained at a higher level compared with the sham-opened group. These results demonstrated that IFITM1 is expressed at the protein level with a spatiotemporally increasing pattern in the spinal cords of sham-operated and injured animals.

In the normal adult spinal cord, the resident cells mainly include astrocytes, neurons, microglia, and oligodendroglia.[19,20] After SCI, there are functional changes of resident cells and the infiltration of leukocytes in the lesion microenvironment.[21–25] These activated cells can produce interferon (IFN)-γ, tumor necrosis factor (TNF)-α, interleukin (IL)-1β, IL-6, and other acute-phase cytokines.[26–28] Therefore, we speculate that the increased expression of IFITM1 in the injured spinal cords might be induced by some of these acute-phase cytokines. Next, we used NeuN, GFAP, APC, CD68, and CD45 to label neurons,[29] astrocytes,[30] oligodendroglia,[31] activated microglia/macrophages,[32] and infiltrated total leukocytes,[33] respectively. Double-immunofluorescence staining showed that IFITM1 was expressed in $GFAP^+$ and APC^+ cells in sham-opened spinal cords. After SCI, it could be found in $CD45^+$, $CD68^+$, $GFAP^+$, and APC^+ cells. Although, some literature reported that IFITM1 can be found in CD45-positive inflammatory cells, CD68-positive macrophages/activated microglia, and astrocytes,[34–36] there were no reports about its expression in normal and injured spinal cords. In the present study, for the first time to our knowledge, we report that IFITM1 is mainly expressed in astrocytes and oligodendroglia in normal spinal cords, and could rapidly increase in infiltrated leukocytes, activated microglia, and astrocytes after SCI. The results of qRT-PCR and western blot showed that in the subacute phase of SCI (7 and 14 dpi), the level of IFITM1 expression is the highest. These results are consistent with the changes of cell types, quantity, and function in the lesion microenvironment, because both leukocyte infiltration and glial activation are peaked at the subacute phase of SCI.[17,37–39] This suggests that the increased expression of IFITM1 may be related to the interferon pathway in infiltrated leukocytes, activated microglia, and astrocytes in the neuroinflammation and neurodegeneration.[40–42]

In summary, our results demonstrate that IFITM1 is mainly expressed in astrocytes and oligodendroglia in normal spinal cords, and could rapidly increase in infiltrated leukocytes, activated microglia, and astrocytes after SCI. These data suggest that IFITM1 may be involved in the pathological process of SCI through the interferon-related signal pathway and is a potential target for treatment of SCI.

Competing Interests

The author(s) declared no potential conflicts of interest with respect to the research, authorship, and/or publication of this article.

Author Contributions

All authors have contributed to this article as follows: H-ZL and J-GH participated in the design and coordination of the study, and drafted the manuscript;YIW, Y-HL, and YAW performed animal experimental procedures, immunohistochemical analyses, and western blot; Z-FY, JT, RW, and LS conducted quantitative reverse transcription-PCR and assisted in data analysis and interpretation; S-QD conceived of the study, participated in its design, and helped draft the manuscript. All authors read and approved the final manuscript.

Funding

The author(s) disclosed receipt of the following financial support for the research, authorship, and/or publication of this article: This study was supported by grants from the National Natural Science Foundation of China (Nos. 81571194, 81471277) and Key Program of Anhui Province for Outstanding Talents in University (Nos. gxbjZD2016071, 2014H012).

Literature Cited

1. Devivo MJ. Epidemiology of traumatic spinal cord injury: trends and future implications. Spinal Cord. 2012;50(5):365–72.
2. Qiu J. China Spinal Cord Injury Network: changes from within. Lancet Neurol. 2009;8(7):606–07.
3. Gwak YS, Kim HY, Lee BH, Yang CH. Combined approaches for the relief of spinal cord injury-induced neuropathic pain. Complement Ther Med. 2016;25:27–33.
4. Shi LL, Zhang N, Xie XM, Chen YJ, Wang R, Shen L, Zhou JS, Hu JG, Lu HZ. Transcriptome profile of rat

genes in injured spinal cord at different stages by RNA-sequencing. BMC Genomics. 2017;18(1):173.
5. Lewin AR, Reid LE, McMahon M, Stark GR, Kerr IM. Molecular analysis of a human interferon-inducible gene family. Eur J Biochem. 1991;199(2):417–23.
6. Sato S, Miller AS, Howard MC, Tedder TF. Regulation of B lymphocyte development and activation by the CD19/CD21/CD81/Leu 13 complex requires the cytoplasmic domain of CD19. J Immunol. 1997;159(7):3278–87.
7. Hatano H, Kudo Y, Ogawa I, Tsunematsu T, Kikuchi A, Abiko Y, Takata T. IFN-induced transmembrane protein 1 promotes invasion at early stage of head and neck cancer progression. Clin Cancer Res. 2008;14(19):6097–105.
8. Sari IN, Yang YG, Phi LT, Kim H, Baek MJ, Jeong D, Kwon HY. Interferon-induced transmembrane protein 1 (IFITM1) is required for the progression of colorectal cancer. Oncotarget. 2016;7(52):86039–50.
9. Yang Y, Lee JH, Kim KY, Song HK, Kim JK, Yoon SR, Cho D, Song KS, Lee YH, Choi I. The interferon-inducible 9-27 gene modulates the susceptibility to natural killer cells and the invasiveness of gastric cancer cells. Cancer Lett. 2005;221(2):191–200.
10. Yu F, Ng SS, Chow BK, Sze J, Lu G, Poon WS, Kung HF, Lin MC. Knockdown of interferon-induced transmembrane protein 1 (IFITM1) inhibits proliferation, migration, and invasion of glioma cells. J Neurooncol. 2011;103(2):187–95.
11. Tanaka SS, Yamaguchi YL, Tsoi B, Lickert H, Tam PP. IFITM/Mil/fragilis family proteins IFITM1 and IFITM3 play distinct roles in mouse primordial germ cell homing and repulsion. Dev Cell. 2005;9(6):745–56.
12. Wylie C. IFITM1-mediated cell repulsion controls the initial steps of germ cell migration in the mouse. Dev Cell. 2005;9(6):723–24.
13. Bailey CC, Zhong G, Huang IC, Farzan M. IFITM-family proteins: the cell's first line of antiviral defense. Annu Rev Virol. 2014;1:261–83.
14. Diamond MS, Farzan M. The broad-spectrum antiviral functions of IFIT and IFITM proteins. Nat Rev Immunol. 2013;13(1):46–57.
15. Lu HZ, Xu L, Zou J, Wang YX, Ma ZW, Xu XM, Lu PH. Effects of autoimmunity on recovery of function in adult rats following spinal cord injury. Brain Behav Immun. 2008;22(8):1217–30.
16. Pfaffl MW. A new mathematical model for relative quantification in real-time RT-PCR. Nucleic Acids Res. 2001;29(9):e45.
17. Chen YJ, Zhu H, Zhang N, Shen L, Wang R, Zhou JS, Hu JG, Lu HZ. Temporal kinetics of macrophage polarization in the injured rat spinal cord. J Neurosci Res. 2015;93(10):1526–33.
18. Drury JA, Nik H, van Oppenraaij RH, Tang AW, Turner MA, Quenby S. Endometrial cell counts in recurrent miscarriage: a comparison of counting methods. Histopathology. 2011;59(6):1156–62.
19. Lecca D, Ceruti S, Fumagalli M, Abbracchio MP. Purinergic trophic signalling in glial cells: functional effects and modulation of cell proliferation, differentiation, and death. Purinergic Signal. 2012;8(3):539–57.
20. Miyagi M, Mikawa S, Sato T, Hasegawa T, Kobayashi S, Matsuyama Y, Sato K. BMP2, BMP4, noggin, BMPRIA, BMPRIB, and BMPRII are differentially expressed in the adult rat spinal cord. Neuroscience. 2012;203:12–26.
21. David S, Greenhalgh AD, Kroner A. Macrophage and microglial plasticity in the injured spinal cord. Neuroscience. 2015;307:311–18.
22. Gordh T, Chu H, Sharma HS. Spinal nerve lesion alters blood-spinal cord barrier function and activates astrocytes in the rat. Pain. 2006;124(1–2):211–21.
23. Karimi-Abdolrezaee S, Billakanti R. Reactive astrogliosis after spinal cord injury-beneficial and detrimental effects. Mol Neurobiol. 2012;46(2):251–64.
24. Popovich PG, Wei P, Stokes BT. Cellular inflammatory response after spinal cord injury in Sprague-Dawley and Lewis rats. J Comp Neurol. 1997;377(3):443–64.
25. Wang L, Hu B, Wong WM, Lu P, Wu W, Xu XM. Glial and axonal responses in areas of Wallerian degeneration of the corticospinal and dorsal ascending tracts after spinal cord dorsal funiculotomy. Neuropathology. 2009;29(3):230–41.
26. Garcia E, Aguilar-Cevallos J, Silva-Garcia R, Ibarra A. Cytokine and growth factor activation in vivo and in vitro after spinal cord injury. Mediators Inflamm. 2016;2016:9476020.
27. Hayashi M, Ueyama T, Nemoto K, Tamaki T, Senba E. Sequential mRNA expression for immediate early genes, cytokines, and neurotrophins in spinal cord injury. J Neurotrauma. 2000;17(3):203–18.
28. Saghazadeh A, Rezaei N. The role of timing in the treatment of spinal cord injury. Biomed Pharmacother. 2017;92:128–39.
29. Mullen RJ, Buck CR, Smith AM. NeuN, a neuronal specific nuclear protein in vertebrates. Development. 1992;116(1):201–11.
30. Eng LF, Ghirnikar RS, Lee YL. Glial fibrillary acidic protein: GFAP-thirty-one years (1969-2000). Neurochem Res. 2000;25(9–10):1439–51.
31. Lebrun-Julien F, Bachmann L, Norrmen C, Trotzmuller M, Kofeler H, Ruegg MA, Hall MN, Suter U. Balanced mTORC1 activity in oligodendrocytes is required for accurate CNS myelination. J Neurosci. 2014;34(25):8432–48.
32. Holness CL, Simmons DL. Molecular cloning of CD68, a human macrophage marker related to lysosomal glycoproteins. Blood. 1993;81(6):1607–13.
33. Harvath L, Balke JA, Christiansen NP, Russell AA, Skubitz KM. Selected antibodies to leukocyte common antigen (CD45) inhibit human neutrophil chemotaxis. J Immunol. 1991;146(3):949–57.
34. Ranjbar S, Haridas V, Jasenosky LD, Falvo JV, Goldfeld AE. A role for IFITM proteins in restriction of mycobacterium tuberculosis infection. Cell Rep. 2015;13(5):874–83.
35. Seyfried NT, Huysentruyt LC, Atwood JA 3rd, Xia Q, Seyfried TN, Orlando R. Up-regulation of NG2 proteoglycan and interferon-induced transmembrane proteins 1 and

3 in mouse astrocytoma: a membrane proteomics approach. Cancer Lett. 2008;263(2):243–52.
36. Tymoszuk P, Charoentong P, Hackl H, Spilka R, Muller-Holzner E, Trajanoski Z, Obrist P, Revillion F, Peyrat JP, Fiegl H, Doppler W. High STAT1 mRNA levels but not its tyrosine phosphorylation are associated with macrophage infiltration and bad prognosis in breast cancer. BMC Cancer. 2014;14:257.
37. Gadani SP, Walsh JT, Lukens JR, Kipnis J. Dealing with danger in the CNS: the response of the immune system to injury. Neuron. 2015;87(1):47–62.
38. Tian DS, Dong Q, Pan DJ, He Y, Yu ZY, Xie MJ, Wang W. Attenuation of astrogliosis by suppressing of microglial proliferation with the cell cycle inhibitor olomoucine in rat spinal cord injury model. Brain Res. 2007;1154:206–14.
39. Wu Y, Lin YH, Shi LL, Yao ZF, Xie XM, Jiang ZS, Tang J, Hu JG, Lu HZ. Temporal kinetics of CD8+ CD28+ and CD8+ CD28– T lymphocytes in the injured rat spinal cord. J Neurosci Res. 2017;95(8):1666–76.
40. Endo F, Komine O, Fujimori-Tonou N, Katsuno M, Jin S, Watanabe S, Sobue G, Dezawa M, Wyss-Coray T, Yamanaka K. Astrocyte-derived TGF-beta1 accelerates disease progression in ALS mice by interfering with the neuroprotective functions of microglia and T cells. Cell Rep. 2015;11(4):592–604.
41. Nikodemova M, Watters JJ, Jackson SJ, Yang SK, Duncan ID. Minocycline down-regulates MHC II expression in microglia and macrophages through inhibition of IRF-1 and protein kinase C (PKC)alpha/betaII. J Biol Chem. 2007;282(20):15208–16.
42. Taylor JM, Moore Z, Minter MR, Crack PJ.Type-I interferon pathway in neuroinflammation and neurodegeneration: focus on Alzheimer's disease. J Neural Transm (Vienna). 2017. Epub 2017 Jul 4. https://doi.org/10.1007/s00702-017-1745-4.